Transport properties of composite solid films with rough self-affine surfaces

Ehsan Nedaaee Oskoee[1] and Muhammad Sahimi[2,*]
[1]*Institute for Advanced Studies in Basic Sciences, Gava Zang, Zanjan 45195-1159, Iran*
[2]*Mork Family Department of Chemical Engineering and Materials Science, University of Southern California, Los Angeles, California 90089-1211*

(Received 12 May 2006; revised manuscript received 26 May 2006; published 13 July 2006)

We develop a method for computing the ac and dc conductivity σ_e of composite films, composed of two types of particles. The films are grown by integrating the Kardar-Parisi-Zhang and the Ginzburg-Landau equations that govern their height and the order parameter. σ_e is computed as a function of the film's thickness, frequency, and several relevant morphological parameters. Simulations indicate that the surface roughness strongly affects the films' conductivity. In particular, while σ_e exhibits universality if the films' surface is smooth, the universality breaks down with a rough surface. The results also indicate the consistency of the trends in the conductivities with the morphological transitions in the films.

DOI: 10.1103/PhysRevB.74.045413 PACS number(s): 68.55.−a, 64.60.Cn, 05.70.Jk, 72.20.−i

I. INTRODUCTION

Heterogeneous solid films (SFs) are used as low-dielectric constant composites, optical coatings, sensors, and insulating materials, and, therefore, their preparation and characterization with specific electronic, optical, and mechanical properties have been studied for a long time.[1] Their growth, usually by molecular beam epitaxy (MBE) or vapor deposition,[2] involves a variety of complex phenomena on two-dimensional (2D) substrates, including nucleation, aggregation, and coalescence of islands on two-dimensional substrates. In MBE, for example, particles are deposited[2] on a substrate through a directed beam, which then diffuse on the surface until they reach energetically favorable positions. These processes lead, in the submonolayer and early multilayer growth, to the formation of a distribution islands of various sizes. The morphology of the islands, which grow and join with the process time, depends on a variety of microscopic details of the growth process, such as the deposition rate, temperature, surface diffusion, and the surface structure of the substrate. For this reason, what happens in the submonolayer regime has important consequences for multilayer growth.

Deposition of only one type of particle may not generate a SF with the desirable electrical and optical properties, which is also mechanically stable and strong. For example, coverage by the incoming particles of a deposited particle which is not, however, in an energetically favorable state, leads to the film's surface being at a steady but not in equilibrium state.

Therefore, it is a common practice to grow *composite* solid films (CSFs) with more than one type of particle. Studies of formation of such CSFs indicate that their growth gives rise to interesting and nontrivial problems. For example, if a set of two types of particles is deposited on a substrate that tend to phase separate on the surface, the resulting film has lamellae or columns of the two phases that are more or less parallel to the direction of film growth.[3] The phase separation phenomenon depends on several factors, including the elastic forces, the orientation of the growing crystal, and the morphology of the substrate on which the films are grown.

A key feature of both the SFs and CSFs is that, as their height or thickness increases, their surface roughens since the layer-by-layer growth mode underlying the process is unstable. The rough surface is typically self-affine and is characterized by a roughness exponent α, defined[4] by

$$C(r) \sim r^{2\alpha}, \tag{1}$$

where $C(r)$ is a front-front correlation function defined by

$$C(r) = \langle [d(x) - d(x+r)]^2 \rangle, \tag{2}$$

with $d(x)$ being the position of a point on the surface (its distance along the growth direction from the substrate) at x, and the averaging, for each value of r (also a point on the surface), is over all values of x. One goal of this paper is to show that surface roughness of SFs strongly influences their transport properties.

A variety of models have been suggested for CSFs that contain both phase separation and surface roughness. For example, a variant of the Eden model[5] was suggested by Ausloos *et al.*[6] They used two types of particles to grow a composite film which led to film surface being rougher than what one obtains with the Eden model with one type of particle. Kotrla and co-workers[7] developed a solid-on-solid growth model in which the sticking probability for the incoming particles depended on the local neighbourhood in the layer below the surface. Their model also led to increased surface roughness, since the incoming particles are more likely to attach themselves to the growing film within the domains or clusters than to their boundaries. Desai and co-workers[8] proposed a model for the growth of thin composite films by a MBE process, made of two types of particles, say A and B. In their model, the incoming particles attach themselves randomly to the growing surface and then diffuse along the surface. This leads to phase separation and domain formation with a thickness which is a nonmonotonic function of the deposition rate and the temperature.

Drossel and Kardar (DK)[9] proposed a set of two Langevin-type equations that couple the films' height to the order parameter's fluctuations. They studied their model in high dimensions using renormalization group calculations, and developed a discrete analog of the model and investigated its properties by computer simulations. Interesting re-

sults were obtained, including a roughness exponent at the critical point of the order parameter which, compared to the disordered phase, was larger. We recently studied[10] the DK model using direct numerical integration and reported several interesting morphological transitions in the films as the model's relevant parameters are varied.

Although many models for the morphology of the SFs and CSFs have been studied, their transport and optical properties, which are important to their use in practice, have not been modeled. Such properties, and in particular the ac and dc conductivities, depend on the films' constituents and the mechanism(s) by which they are distributed in the films' matrix.[11,12] Moreover, the films' rough surface induces additional electron scattering,[13] which may affect the transport properties.

In this paper we develop and study a model for computing the ac and dc electrical conductivity of the CSFs grown by the DK model which, to our knowledge, has never been attempted before. The model and the computational techniques that we describe in this paper are, however, general and may be used with any other model of growth of the CSFs. The optical properties are usually expressed in terms of the material's dielectric constant,[11] modeling of which is similar to the conductivity.

The plan of this paper is as follows. In Sec. II we describe the continuum DK model which is utilized in this paper for the growth of the CSFs, and how it is integrated. Section III presents the transport model that we utilize for computing the films' ac and dc conductivity. In Sec. IV we describe the computational techniques that we use to calculate the films' ac and dc electrical conductivity. The results are then presented and discussed in Sec. V. We summarize the paper in Sec. VI.

II. MODEL OF FILM GROWTH

In the DK model, which is intended for growth of the CSFs by vapor deposition, phase separation is characterized by an order parameter $m(\mathbf{x},t)$ that represents the difference between the densities of the A and B particles at position $\mathbf{x}$ at time t. The growth of the surface height $h(\mathbf{x},t)$ is described by

$$\frac{\partial h}{\partial t} = \nu\nabla^2 h + \frac{1}{2}\lambda(\nabla h)^2 + \frac{1}{2}\chi m^2 + \eta_h(\mathbf{x},t), \tag{3}$$

which is the Kardar-Parisi-Zhang (KPZ) equation,[14] together with a coupling term. Here, η_h represents thermal fluctuations of the particles' flux with

$$\langle \eta_h(\mathbf{x},t)\cdot\eta_h(\mathbf{x}',t')\rangle = 2D_h\delta^d(\mathbf{x}-\mathbf{x}')\delta(t-t'), \tag{4}$$

where D_h is the noise's amplitude, and d is the film's spatial dimension. The order parameter $m(\mathbf{x},t)$ is governed by the time-dependent Ginzburg-Landau (GL) equation, together with several terms that couple it to the KPZ equation

$$\frac{\partial m}{\partial t} = K(\nabla^2 m + rm - um^3) + a\,\nabla h\cdot\nabla m + bm\nabla^2 h + \frac{1}{2}cm(\nabla h)^2 + \eta_m(\mathbf{x},t). \tag{5}$$

Here, η_m represents the fluctuations in the density of the particles, defined in a manner similar to $\eta_h(\mathbf{x},t)$ with an amplitude D_m. The coupling terms are derived by symmetry arguments.[9] The model described by Eqs. (3)–(5) was derived by Kardar[9] based on a discrete model that satisfies detailed balance, the order parameter of which was shown to be described, in the continuum limit, by Eq. (5). Unlike models of growth of the SFs,[4] the signs and magnitudes of the coupling parameters χ, a, and c, affect the model's scaling properties[10] and, hence, we also consider their effect on the transport properties.

In order to grow the CSFs using the DK model, we first rewrite Eqs. (3) and (5) in dimensionless form. To do so, we note that the amplitudes D_h and D_m have different dimensions ($[D_h]\equiv L^3t^{-1}$ and $[D_m]\equiv Lt^{-1}$). Hence, we utilize them to rewrite Eqs. (3) and (5) in dimensionless forms by defining

$$\begin{aligned}
\tilde{x} &= x\sqrt{\frac{D_m}{D_h}} & \tilde{K} &= \frac{K}{\sqrt{D_m D_h}}\\
\tilde{t} &= tD_m\sqrt{\frac{D_m}{D_h}} & \tilde{r} &= r\frac{D_h}{D_m}\\
\tilde{h} &= h\sqrt{\frac{D_m}{D_h}} & \tilde{u} &= u\frac{D_h}{D_m}\\
\tilde{\nu} &= \frac{\nu}{\sqrt{D_m D_h}} \quad \text{and} & \tilde{a} &= \frac{a}{D_m}\\
\tilde{\lambda} &= \frac{\lambda}{D_m} & \tilde{b} &= \frac{b}{D_m}\\
\tilde{\chi} &= \frac{\chi}{D_m} & \tilde{c} &= \frac{c}{D_m}\sqrt{\frac{D_h}{D_m}}
\end{aligned} \tag{6}$$

which yield a set of two dimensionless equations that are identical in forms to Eqs. (3) and (5), except that the noise amplitudes in the dimensionless forms are 2 (instead of $2D_m$ or $2D_h$).

We then discretize the dimensionless versions of Eqs. (3) and (5) with a fully implicit finite-difference (FD) method. The resulting set of discretized nonlinear equations are solved (in conjunction with the transport model; see below) using the Newton-Raphson and biconjugate-gradient methods. The coupled equations were integrated up to the time $t=10^3$ with a dimensionless time step $\Delta t=0.1$. The Gaussian noises η_h and η_m, were generated using the Box-Muller transformation.[15] The simulations were carried out for a grid (the line on which the film is grown) size $L=1024$. We made many realizations for each case, and averaged the results over all the realizations.

We should emphasize that the numerical integration of Eqs. (3) and (5) is not straightforward and, in particular, the convergence of their solutions to the asymptotic (long-time)

regime can be very slow, if the numerical values of the various coefficients are not selected carefully. For example, instead of using a dimensionless noise amplitude of 2 in the dimensionless GL equation, one may adjust its numerical value in order to speed up the computation of the solution of the two equations. The reason is that in the GL equation the parameter r and the noise amplitude η_m both affect the system's temperature. Thus, varying r requires also adjusting the noise amplitude in the GL equation. In particular, if r is reduced, so should also be the noise amplitude. Otherwise, the asymptotic regime will be reached very slowly, making the computations intractable. More details of the numerical integration of Eqs. (3) and (5) and the tests that we carried out in order to ensure the accuracy of the solution, are given elsewhere.[10]

III. THE TRANSPORT MODEL

To compute the films' ac and dc conductivity, we assume that they are characterized by a *local* frequency-independent conductivity $g(\mathbf{x})$, and a uniform dielectric constant ϵ_∞, so that the current density is given by

$$\mathbf{J}(\mathbf{x},t) = -g(\mathbf{x})\,\nabla\,\phi(\mathbf{x},t) \tag{7}$$

and the displacement field by

$$\mathbf{D}(\mathbf{x},t) = -\epsilon_\infty\,\nabla\,\phi(\mathbf{x},t), \tag{8}$$

where ϕ is the electrostatic potential. Combining these equations with the Gauss' law

$$\nabla\cdot\mathbf{D}(\mathbf{x},t) = \rho(\mathbf{x},t), \tag{9}$$

where ρ is the free charge carrier density, and the continuity equation

$$\frac{\partial\rho}{\partial t} + \nabla\cdot\mathbf{J}(\mathbf{x},t) = 0, \tag{10}$$

we obtain

$$\nabla\cdot\left[\epsilon_\infty\frac{\partial}{\partial t}\phi(\mathbf{x},t) + g(\mathbf{x})\,\nabla\,\phi(\mathbf{x},t)\right] = 0. \tag{11}$$

Since in a periodically-varying field all quantities are written as functions of $\mathbf{x}$ times $\exp(i\omega t)$, we obtain[11,16]

$$\nabla\cdot\{[s+g(\mathbf{x})]\,\nabla\,\phi(\mathbf{x},s)\} = 0, \tag{12}$$

where $s=i\omega\epsilon_\infty$. The discretized form of Eq. (12) is then solved by the method described below. Each block in the computational grid that we obtain from discretization of Eqs. (3) and (5) by a FD method is characterized by an admittance $y=\beta(s+g)=\beta(i\omega\epsilon_\infty+g)$, where β is a constant. The block's conductivity g depends on its composition (fractions of the A and B particles), the estimation of which is described below. If the overall admittance of the d-dimensional material of thickness h is $Y(s)$, its effective ac conductivity $\sigma_e(s)$ is given by[11,16]

$$\sigma_e(s) = \frac{h}{(h+1)^{d-1}}Y(s) - s. \tag{13}$$

Note that, the effective conductivity σ_e so computed is a complex function, as $s=i\omega\epsilon_\infty$.

IV. COMPUTING THE ELECTRICAL CONDUCTIVITY

To compute the effective frequency-dependent conductivity $\sigma_e(s,t_1)$ of the films we solve the discrete version of Eq. (12) in a computational grid, which is constructed based on the FD grid used for integrating Eqs. (3) and (5), up to time t_1. The procedure for constructing this grid is described below. Film growth is then continued by integrating Eqs. (3) and (5) up to time $t=t_2>t_1$ and thickness h_2, based on which $\sigma_e(s,t_2)$ is computed, and so on.

Every block in the grid obtained from FD discretization of Eqs. (3) and (5) is characterized by the densities of the particles A and B that it contains, hence representing a mesoscopic portion of the material at the scale of the block's size. To solve Eq. (12) one must first compute the grid blocks' conductivities $g(\mathbf{x})$. We assume that in every grid block particles A and B (conductivities g_A and g_B) are distributed randomly, an assumption that may be relaxed. The problem at the blocks' scale is thus reduced to computing the conductivity of random binary mixtures that make the blocks. To do so, we use the effective-medium approximation (EMA) which has proven[11,12] to be accurate under a variety of conditions, especially in 2D. (When the domains' shape is important, as when phase separation occurs, one may use the differential EMA (Refs. 11 and 12) which, to some extent, takes into account the shape's effect.) If a 2D material consists of two phases with constant conductivities (g_1,g_2) and volume fractions or densities (v_1,v_2), its effective conductivity g is predicted by the EMA to be the root of

$$\sum_{i=1}^{2} v_i\frac{g_i-g}{g_i+g} = 0. \tag{14}$$

We used $g_A=g_1=2$ and $g_B=g_2=0.1$, but other values may be used as well. This generates the spatial distribution of the blocks' conductivities $g(\mathbf{x})$.

The grid's size, especially at intermediate and long times, is very large. The substrate's linear size is $L=1024$, while in the vertical direction, along which the film grows, the size at long times is about the same, hence implying that, at intermediate and long times, we must solve over a million equations at each time step.[17] To reduce the computations, we coarsen the grid by a method somewhat similar to what was recently introduced.[18]

Briefly, if in any region of the grid the blocks' conductivities are very low, or if they are not much different from one another, there is no need for having a detailed grid structure in that region. Thus, we merge such blocks to obtain a larger block, and compute its effective conductivity based on those of the individual smaller blocks that make up the larger one, using the usual laws of conductors in series or parallel configuration, or a small resistor network. This generates a coarsened computational grid with far fewer blocks, the conductivity σ_e of which at times $t_1,t_2,\ldots$, is computed.

Due to the coarsening, the blocks' sizes are not necessarily the same everywhere.[18] Therefore, we utilized the finite-volume (FV) method.[18,19] In this method one first integrates the equations over the system's volume, and invokes the di-

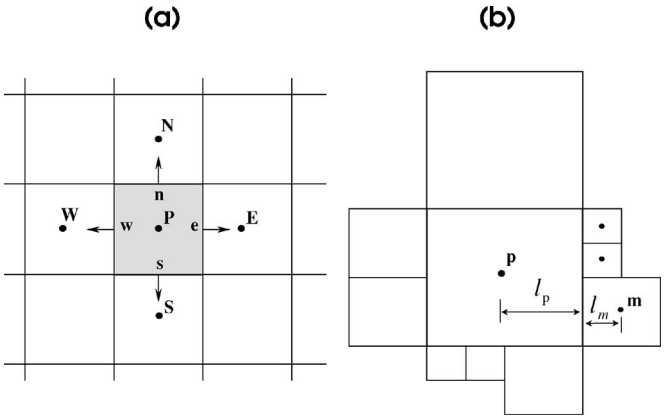

FIG. 1. (a) A typical CV and its neighbors. (b) Neighboring grid blocks of different sizes.

vergence theorem to convert the volume integrals to surface integrals

$$\int_V \nabla \cdot \{[s+g(\mathbf{x})]\nabla \phi(\mathbf{x},s)\}dv = \int_{\partial V} [s+g(\mathbf{x})]\nabla \phi(\mathbf{x},s)\cdot d\mathbf{A} = 0, \tag{15}$$

where $d\mathbf{A}$ is the surface element and ∂V represents the system's surface. The net flux through a square grid block is the sum of the integrals over its four faces,[18–20]

$$\int_{\partial V} \mathbf{J}dA \simeq \sum_{k=1}^{4} \mathbf{J}A_k, \tag{16}$$

where $\mathbf{J}$ is the flux in the direction normal to the block's face. As each block's conductivity g has already been computed (see above), the only remaining unknown is the electrostatic potential $\phi(\mathbf{x},t)$ and its gradient normal to the blocks' faces on their surface [Fig. 1(a)].

To compute the electrostatic potential and its gradient, we use the linear interpolation which is used most commonly.[20] At e [Fig. 1(a)], for example, we have, $\phi_e=\phi_E\lambda_e+\phi_p(1-\lambda_e)$ with, $\lambda_e=(x_e-x_p)/(x_E-x_p)$, which is of second-order accuracy. Moreover, $(\partial\phi/\partial x)_e \simeq (\phi_E-\phi_p)/(x_E-x_p)$. Thus, for the typical configuration of the blocks shown in Fig. 1(b), we obtain[18,21]

$$\int_{\partial v} [s+g(\mathbf{x})]\nabla \phi(\mathbf{x},s)\cdot d\mathbf{A} = \sum_{n=1}^{N}\sum_{m=1}^{M}(s+g_{pm})\left(\frac{\phi_p-\phi_m}{l_p+l_m}\right)\Delta A_m = 0, \tag{17}$$

where N is the number of common faces that each block has with other blocks, M the number of neighbors in each face, ΔA_m the common surface betwen two neighboring blocks, and g_{pm} the equivalent conductivity between the two nodes representing the two neighboring blocks [Fig. 1(b)] given by

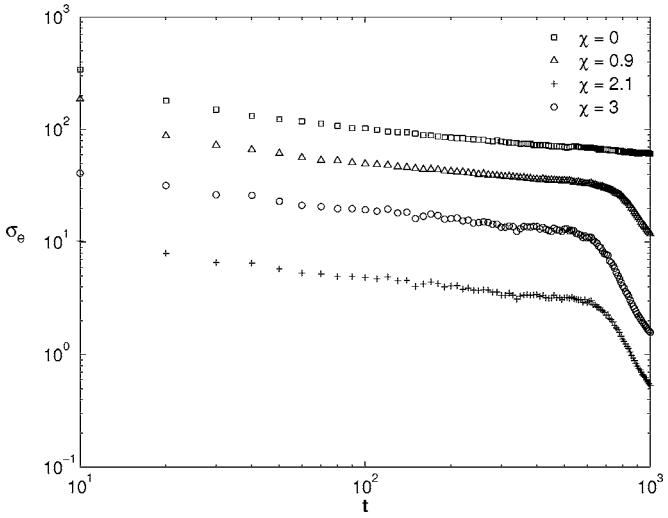

FIG. 2. Dependence of the conductivity $\sigma_e(s)$ on t for four values of the coupling parameter χ and $s=1$.

$$g_{pm} = \frac{l_p+l_m}{l_p/g_p+l_m/g_m}. \tag{18}$$

The set of equations resulting from applying Eq. (17) to every block and its faces is then solved by the biconjugate-gradient method.[17]

V. RESULTS AND DISCUSSIONS

As we showed previously, the parameter b of Eq. (5) does not have any important effect on the dynamics of the GL equation. Thus, one may expect b to have no significant effect on the *qualitative* behavior of the effective conductivity σ_e (the numerical value of σ_e does, of course, depend on b), which is indeed the case.[17] On the other hand, whereas we showed previously[10] that the parameter a of Eq. (5) does affect the dynamics of the GL equation, we find that it has no important effect on the qualitative behavior of σ_e. The reason is that the dynamics of the GL equation is influenced by the dynamics of the domain walls (which is influenced by the parameter a), but *at* the domain walls the two components' densities are *equal* and, therefore, the order parameter m is zero. On the other hand, the effective conductivity is influenced, at low or zero frequency, by disorder in the material, i.e., by the regions in which the density of one component is larger than that of the other. That is, the effective conductivity is influenced by the regions *in between* the domain walls, not the domain walls themselves. This is indeed what we find.[17]

We showed previously[10] that varying χ gives rise to nonuniversal roughness exponent α. In Fig. 2, we show $\sigma_e(s,t)$ as a function of the time t for $a=b=c=0$ and $s=1.0$. σ_e decreases with t, i.e., as the film grows and its surface roughens. At a crossover time t_χ the decrease in σ_e suddenly accelerates. t_χ corresponds *precisely* to the crossover time that we previously identified[10] as the time at which the film's width suddenly increases faster and surface roughening accelerates.

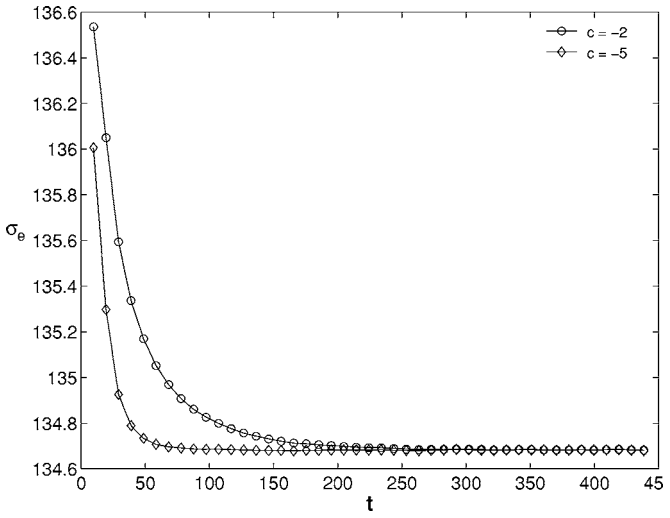

FIG. 3. Time dependence of the effective conductivity σ_e for $c<0$. In this case, the effective conductivity sharply decreases as the film grows.

It is known that in the KPZ model ($\chi=0$), the growth of the film's height saturates after a crossover time $t_\times$ and, hence, the surface roughness becomes fixed, implying that σ_e should also saturate. However, as we showed previously,[10] for $\chi\neq 0$ and times $t>t_\times$, Eq. (1) simplifies to (other terms become unimportant), $\partial h/\partial t \simeq \frac{1}{2}\chi m^2+\eta_h(\mathbf{x},t)$ and, therefore, not only does the film's surface roughen greatly, but also does not saturate. Hence, σ_e should not also saturate, which is what Fig. 2 indicates.

For $c<0$ the film's morphology suddenly switches to a disordered regime at a characteristic time t_c.[10] Correspondingly, σ_e reduces with t with the increasing disorder. This is shown in Fig. 3. On the other hand, for $c>0$ the domains saturate and stop growing,[10] implying that σ_e should also saturate, which is indeed what we find. Figure 4 presents the results for $c>0$, which indicates that the effective conductivity saturates for all values c when $c>0$.

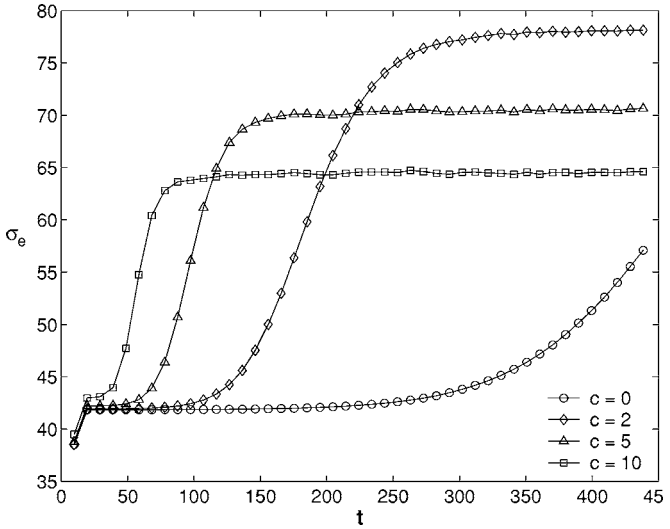

FIG. 4. Same as in Fig. 3, but for $c\geqslant 0$. In this case, the effective conductivity saturates for $c>0$, in agreement with what was found previously[10] for the film's morphology.

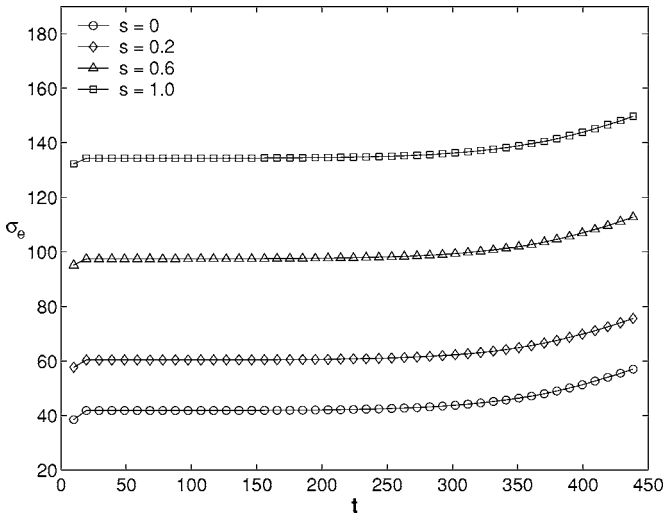

FIG. 5. Frequency and time dependence of the effective conductivity. All the coupling constants are zero.

Figure 5 presents the frequency-dependence of the effective conductivity at various times. As the complex frequency s increases, so also does the conductivity. This trend is in accord with what one expects from the transport model described in Sec. III.[11,16,18,22] To understand better the differences between the various curves of Fig. 5, we rescale the conductivities by their values at $t\simeq 20$, when the film has grown enough to have a significant conductivity. The results are shown in Fig. 6. At early times, all the conductivities collapse onto one another, as the capacitance effect is not important yet, because the film's thickness is not yet large. At longer times, however, when the film's thickness is larger, the dc conductivity (in the limit $s=0$) seems to grow fast with the time. Increasing the frequency reduces the effect of the film's morphology by increasing the capacitance effect.

We now address the question of the universality of $\sigma_e(s)$. To do so, two distinct cases are considered. In one, the material's surface roughness is neglected by "peeling away" the

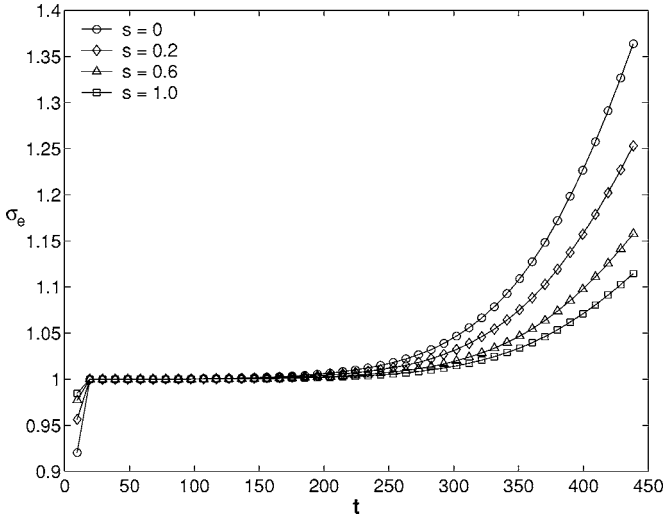

FIG. 6. The conductivities of Fig. 5, now rescaled with their early-time values.

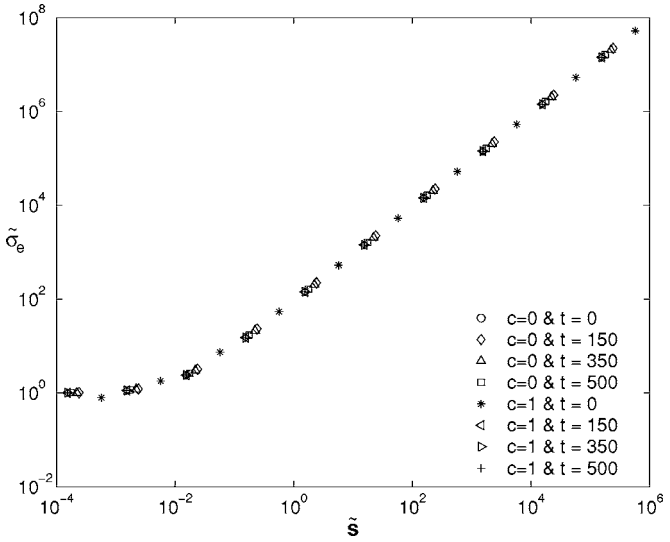

FIG. 7. Universality of the scaled conductivity $\tilde{\sigma}_e$ with the scaled frequency $\tilde{s}$, at various times and values of the coupling constant c. The films' surface is smooth.

roughness and generating a smooth surface (the morphology in the rest of the material remained intact). Then, a constant potential difference is applied between the top and bottom of the material, and $\sigma_e(s,t,\mathbf{p})$ is computed, with $\mathbf{p}=(a,c,\chi)$ being the set of the relevant coupling parameters. In the second case, the surface roughness is not removed, a constant potential is applied at the bottom (on the substrate), and a constant current is extracted from a point in the middle of the rough surface at the top. While the thickness of the roughened area (with "hills" and valleys") at the material's top surface is small compared with its overall height $h(t)$, it has a dramatic effect on the transport properties.

Shown in Fig. 7 is $\tilde{\sigma}_e=\sigma_e(s)/\sigma_e(0)$ versus $\tilde{s}=s/\sigma_e(0)$ for the decoupled case, $a=b=c=0$, as well as $c=1$ at four different times and neglecting the surface roughness. $\tilde{\sigma}_e(\tilde{s})$ is a universal function of $\tilde{s}$ at all times. This universality, found for all values of the coupling parameters a, b, c, and χ,[17] is

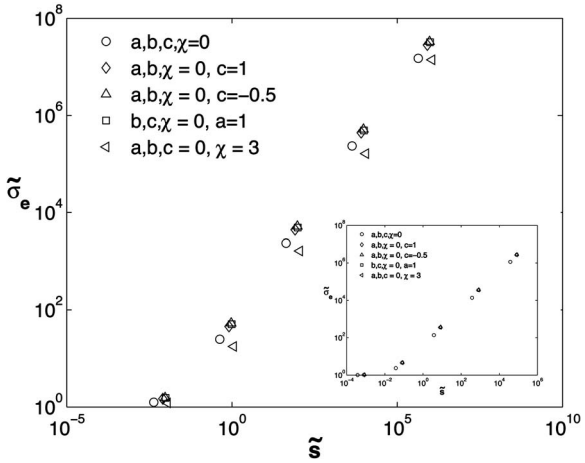

FIG. 8. Nonuniversality of the rescaled conductivity when the films' surface is rough. The inset shows the results when the surface is not rough.

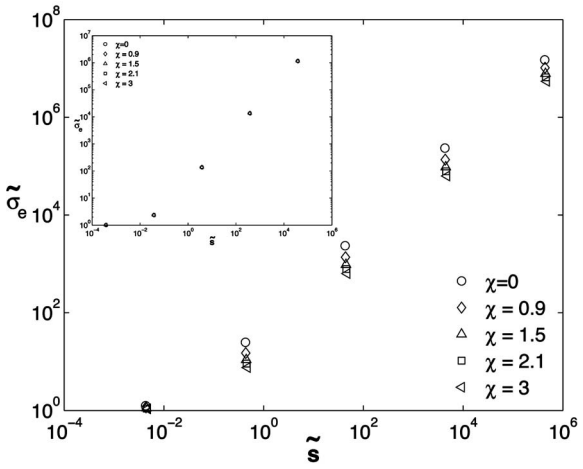

FIG. 9. Universality of the effective conductivity of a film with only one type of particle, when the surface has no roughness (the inset), and when it is rough. Here, $a=b=c=0$.

similar to what has been found for amorphous semiconductors, polymers, and ionically conductive glasses,[11,18,22] although the films that we grow do not have much in common with such materials.

However, when the surface roughness is not neglected, the universality breaks down. Shown in Fig. 8 are the results for this case for several values of the coupling constants and at (dimensionless) time, $t=10^3$, indicating no universality. If, for the same set of parameters, σ_e is computed when there is no surface roughness, the universality is restored; see the inset of Fig. 8.

If we set $g_A=g_B$ to generate a film with only one type of particle, we obtain the same type of results, shown in Fig. 9: When the surface is smooth, the scaled conductivity is a universal function of $\tilde{s}$, but when it is rough, the nonuniversality is restored. Thus, unlike many other materials, the surface roughness of the SFs and CSFs grown by deposition strongly affects their transport (and, hence, optical) properties.

VI. SUMMARY

We presented a general method of computing the effective transport properties of single-component and binary composite films, grown by deposition of one or two types of particles on a substrate. We showed that if the films' surface roughens, then their conductivity $\tilde{\sigma}_e(\tilde{s})$ is a nonuniversal function of the frequency $\tilde{s}$, whereas with a smooth surface $\tilde{\sigma}_e(\tilde{s})$ becomes a universal function of $\tilde{s}$. In addition, we showed that the behavior of the film's conductivity is closely connected with its morphology: Every morphological transition that we had identified previously[10] seem to have a corresponding counterpart in the effective conductivity. Thus, measurement of the film's conductivity should provide crucial cluse to its morphology.

ACKNOWLEDGMENTS

The authors' work was supported, respectively, by the NIOC and DOE.

*Electronic address: moe@iran.usc.edu

[1] B. Lewis and J. C. Anderson, *Nucleation and Growth of Thin Films* (Academic Press, New York, 1978).

[2] *The Technology and Physics of Molecular Beam Epitaxy*, edited by E. H. C. Parker (Plenum, New York, 1985); J. Y. Tsao, *Materials Fundamentals of Molecular Beam Epitaxy* (World Scientific, Singapore, 1993).

[3] T. L. McDevitt, S. Mahajan, D. E. Loughlin, W. A. Bonner, and V. G. Keramidas, Phys. Rev. B **45**, 6614 (1992); C. D. Adams, M. Atzmon, Y.-T. Cheng, and D. J. Srolovitz, J. Mater. Res. **72**, 653 (1992).

[4] *Dynamics of Fractal Surfaces*, edited by F. Family and T. Vicsek (World Scientific, Singapore, 1991); A. L. Barabási and H. E. Stanley, *Fractal Concepts in Surface Growth* (Cambridge University Press, London, 1995); P. Meakin, *Fractals, Scaling and Growth far from Equilibrium* (Cambridge University Press, Cambridge, 1998).

[5] M. Eden, in *Proceedings of the Fourth Berkeley Symposium on Mathematical Statistics and Probability, Volume IV: Biology and Problems of Health*, edited by J. Neyman (University of California Press, Berkeley, 1959), p. 223.

[6] M. Ausloos, N. Vandewalle, and R. Cloots, Europhys. Lett. **24**, 629 (1993).

[7] M. Kotrla and M. Predota, Europhys. Lett. **39**, 251 (1997); M. Kotrla, M. Predota, and F. Slanina, Surf. Sci. **404**, 249 (1998); M. Kotrla, F. Slanina, and M. Predota, Phys. Rev. B **58**, 10003 (1998).

[8] F. Leonard and R. C. Desai, Phys. Rev. B **55**, 9990 (1997); F. Leonard, M. Laradji, and R. C. Desai, *ibid.* **55**, 1887 (1997).

[9] B. Drossel and M. Kardar, Phys. Rev. Lett. **85**, 614 (2000); Eur. Phys. J. B **36**, 401 (2003); M. Kardar, in *Scaling and Disordered Systems*, edited by D. Stauffer, Vol. VIII of Annual Reviews of Computational Physics (World Scientific, Singapore, 2001), p. 1.

[10] E. Nedaaee Oskoee, M. R. H. Khajehpour, and M. Sahimi, Phys. Rev. E **69**, 061606 (2004); E. Nedaaee Oskoee and M. Sahimi, Int. J. Mod. Phys. C **16**, 727 (2005).

[11] M. Sahimi, *Heterogeneous Materials I & II* (Springer, New York, 2003).

[12] S. Torquato, *Random Heterogeneous Materials* (Springer, New York, 2002).

[13] G. Palasantzas and J. Th. M. De Hosson, Phys. Rev. B **63**, 125404 (2001).

[14] M. Kardar, G. Parisi, and Y. C. Zhang, Phys. Rev. Lett. **56**, 889 (1986).

[15] W. H. Press, B. P. Flannery, S. A. Teukolsky, and W. T. Vetterling, *Numerical Recipies*, 2nd ed. (Cambridge University Press, Cambridge, 1992).

[16] J. C. Dyre, Phys. Rev. B **47**, 9128 (1993); **48**, 12511 (1993); **49**, 11709 (1994).

[17] E. Nedaaee Oskoee, Ph.D. thesis, Institute for Advanced Studies in Basic Science, Zanjan, Iran, 2005.

[18] M. Sahimi, M. Naderian, and F. Ebrahimi, Phys. Rev. B **71**, 094208 (2005); E. Pazhoohesh, H. Hamzehpour, and M. Sahimi, *ibid.* **73**, 174206 (2006).

[19] R. J. Leveque, *Finite Volume Methods for Hyperbolic Problems* (Cambridge University Press, Cambridge, 2002).

[20] D. Kim and H. Choi, J. Comput. Phys. **162**, 411 (2000); B. Rogers, M. Fujihara, and A. G. L. Borthwick, Int. J. Numer. Methods Fluids **35**, 247 (2001).

[21] A. Heidarinasab, B. Dabir, and M. Sahimi, Atmos. Environ. **38**, 6381 (2004).

[22] J. C. Dyre and T. B. Schroder, Rev. Mod. Phys. **72**, 873 (2000).